Technical Physics, 2022, Vol. 67, No. 11

15

Quantum magnetometer based on cross-relaxation resonances in ensembles of NV-centers in diamond

© *R.A. Akhmedzhanov, L.A. Gushchin, I.V. Zelensky, A.V. Kupaev, V.A. Nizov, N.A. Nizov, D.A. Sobgayda*

Institute of Applied Physics, Russian Academy of Sciences,
Nizhny Novgorod, Russia
e-mail: zelensky@appl.sci-nnov.ru

Received May 18, 2022
Revised August 12, 2022
Accepted August 14, 2022

We create a working model of a magnetometer of a new type that is based on using cross-relaxation resonances in ensembles of NV-centers in diamond. This type of magnetometer does not require microwave radiation. For a sensor made out of a 300 micron diamond we demonstrate the magnetic field sensitivity of around 18 nT/Hz$^{1/2}$.

Keywords: cross-relaxation, NV-center, quantum magnetometer.

DOI: 10.21883/TP.2022.11.55183.138-22

Introduction

At present, NV-centers in diamond are considered as a promising quantum system for high-sensitivity optical magnetometry [1,2]. Progress in research leads to a gradual transition from laboratory experiments to the creation of working prototypes of quantum magnetometers (see, for example, [3–6]).

A significant disadvantage of the „traditional" NV-center magnetometry scheme based on the observation of optically detected magnetic resonance [1–6], is the need to use microwave radiation (frequency ~ 2.8 GHz). The use of microwave radiation limits the scope of applicability of the method, as in some cases its use can be difficult, for example, near conductive materials, or can lead to undesirable effects on the object of study, for example, in biology and medicine. Because of this, alternative approaches to the implementation of magnetometry with NV-centers are being actively developed. One such option is an approach based on fluorescence reduction in strong (on the order of tens mT) magnetic fields [7–9]. However, this method has a low sensitivity. Another method for implementing magnetometry is based on the effect of anti-crossing of the spin sublevels of the ground state [10,11]. A significant disadvantage of this method is the need to apply a sufficiently strong (on the order of 0.1 T) and precisely oriented magnetic field to the diamond, which complicates the sensor construction and limits the applicability of the magnetometer. There is also a method for measuring the magnetic field using the effects observed when the diamond with NV-centers is exposed to HF radiation (1–10 MHz) [12]. This approach, according to the authors, due to the absence of microwave radiation and the small size of the sensor can become promising for biomedical research. Another fully optical, though rather difficult to implement, method is based on the effects of coherent population trapping and electromagnetically induced transparency [13,14].

Previously, we proposed a method for measuring the magnetic field based on cross-relaxation resonances in an ensemble of NV-centers in diamond [15,16]. The method does not require the use of additional factors, such as strong magnetic field or HF or microwave radiation. The purpose of this work is a practical implementation of the magnetometer model based on this principle.

1. Magnetometer operating principle

NV-centers in diamond have a system of energy levels and transitions (Fig. 1, *a*), in which optical pumping causes predominant occupancy of the $m_s = 0$ spin sublevel of the ground state. The observed fluorescence is also spin-dependent (brighter for $m_s = 0$). The „traditional" scheme of NV-center magnetometry uses the measurement of frequencies of transitions between the ground state sublevels, dependent on magnetic field, by fluorescence reduction when microwave radiation is applied (optically detected magnetic resonance (ODMR) method).

The model uses a method that does not require microwave radiation, based on the observation of cross-relaxation resonances in an ensemble of NV-center [15,16]. The essence of the method is as follows. In a diamond crystal four different directions of the NV-center axis are possible: [1,1,1], [−1, 1, 1], [1, −1, 1], [1, 1, −1] (in the coordinate system associated with the major crystallographic axes (Fig. 1, *b*)). The frequencies of microwave transitions between the ground state sublevels depend on the magnitude of the magnetic field and its projection on the NV-center axis. If the magnetic field has equal moduli of projections onto the axes of two groups of NV-centers, the frequencies of microwave transitions for the two groups coincide. This leads to a cross-relaxation interaction between them and a change in the fluorescence signal.

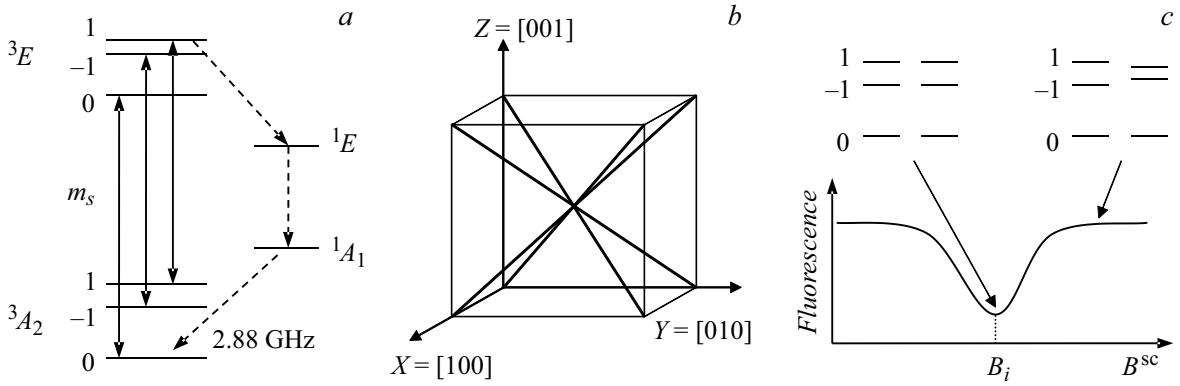

Figure 1. *a* — scheme of NV-center levels, solid arrows show optical transitions between the spin sublevels of the ground — $^3A_2$ and excited — ^3E states with spin projection preservation, dotted arrows show additional relaxation path of $m_s = \pm 1$ sub-levels of excited state without spin projection preservation; *b* — four possible orientations of the NV-center; *c* — cross relaxation resonance, at the center of the resonance the frequencies of transitions between ground state sublevels for two or more groups of differently oriented NV-centers coincide, outside the resonance — do not coincide.

Let the magnetic field be the sum of unknown constant and scanning fields $\mathbf{B}^{\Sigma} = \mathbf{B}^{\mathbf{dc}} + B^{sc}\mathbf{b}^{\mathbf{sc}}$, where $\mathbf{B}^{\mathbf{dc}}$ — the constant magnetic field, B^{sc} — the magnitude of the scanned field, $\mathbf{b}^{\mathbf{sc}}$ — the unit vector in the scan direction. When the transition frequencies for two or more groups of differently oriented NV-centers coincide, cross-relaxation resonance is observed in the fluorescence dependence on the scanned field (Fig. 1, *c*). In the general case, up to nine resonances can be observed, the positions of which are described by the expression:

$$B_i = -(\mathbf{B}^{\mathbf{dc}}, \mathbf{v_i})/(\mathbf{b}^{\mathbf{sc}}, \mathbf{v_i}), \tag{1}$$

where $\mathbf{v_i}$ — vectors [1,0,0], [0,1,0], [0,0,1], [0,1,1], [1,0,1], [1,1,0], [0, −1, 1], [−1, 0, 1], [1, −1, 0].

The positions of the resonances depend on the constant magnetic field and can therefore be used to measure it. Various measurement schemes are possible. We followed a protocol similar to the one outlined in the [16]. The $\mathbf{Z} = [0, 0, 1]$ axis was chosen as the scanning direction (misalignment angles up to 5° are permissible). The dependence of the fluorescence signal on the z-component of the scanned field was measured, respectively the position of the resonances on it $b_i = b_z^{sc} B_i$. With this choice of scanning direction, for four vectors $\mathbf{v_i}$ the denominators in expression (1) are small and the corresponding resonances are not observed, the positions of the other five are given by the expressions

$$b_{[001]} = -B_z^{dc}, \tag{2}$$

$$b_{[101]} = -(B_x^{dc} + B_z^{dc})/(1+\alpha), \tag{3}$$

$$b_{[-101]} = (B_x^{dc} - B_z^{dc})/(1-\alpha), \tag{4}$$

$$b_{[011]} = -(B_y^{dc} + B_z^{dc})/(1+\beta), \tag{5}$$

$$b_{[0-11]} = (B_y^{dc} - B_z^{dc})/(1-\beta), \tag{6}$$

where $\alpha = b_x^{sc}/b_z^{sc}$, $\beta = b_y^{sc}/b_z^{sc}$.

Note that in the area of small magnetic fields the resonances are not split, besides, it is not always possible to unambiguously match the positions of the resonances with the expressions of the system (2)−(6). To overcome these drawbacks, an additional bias magnetic field (see [16]) can be used, which splits the resonances and allows to determine their order. Let x-component of the bias field be greater than y-component and both be positive, in which case the positions of resonances (numbered in ascending order): $b_1 = b_{[101]}$, $b_2 = b_{[011]}$, $b_3 = b_{[001]}$, $b_4 = b_{[0-11]}$, $b_5 = b_{[-101]}$. The measured magnetic field $\mathbf{B}$ leads to a shift of resonances Δ_i. From expressions (2)−(6) we can obtain the following expressions for $\mathbf{B}$:

$$B_z = -\Delta_3, \tag{7}$$

$$B_x = [(1-\alpha)\Delta_5 - (1+\alpha)\Delta_1]/2, \tag{8}$$

$$B_y = [(1-\beta)\Delta_4 - (1+\beta)\Delta_2]/2, \tag{9}$$

The coefficients $\alpha = (b_5 + b_1 - 2b_3)/(b_5 - b_1)$ and $\beta = (b_4 + b_2 - 2b_3)/(b_4 - b_2)$ are also expressed through the resonance positions.

Thus, to measure the magnetic field, it is necessary to measure the positions of the resonances and their shifts relative to the positions corresponding to the zero measured field.

2. Model layout

The photographic image of the model is presented in Fig. 2. The model consists of the optical part *1*, the electronics unit *2* and sensor *3*, as well as the laser *4* and the balanced photodetector *5*. All parts of the model are connected by flexible multimode optical fibers and/or wires and can, if necessary, with minimal rework be placed inside a common enclosure. The model is controlled by a computer (not shown in the illustration).

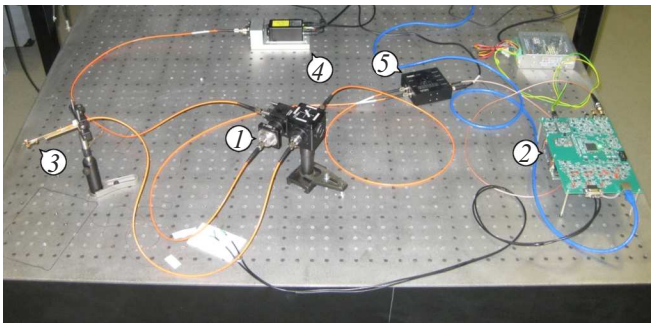

Figure 2. Photo of the model: *1* — optical unit, *2* — electronic unit, *3* — sensor, *4* — laser, *5* — balanced photo detector.

A block diagram of the model is shown in Figure 3, *a*. The optical part of the model (Fig. 3, *a* and photo in 3,*b*) is assembled from Thorlabs elements, which can be connected to each other in various combinations. This approach allowed us to try out different model layout options and choose the optimal configuration.

In Fig. 3 the optical unit is assembled on the basis of two structural cubes CM1-DCH/M and DFM1/M, in which mirrors and filters are mounted. F950FC-A collimators with AD15F adapters and PAF2P-A10A fiber port are used for input and output of radiation from optical fibers. The laser radiation reflected from the DMLP605R dichroic mirror enters the sensor, the fluorescence signal from the sensor passes through the dichroic mirror, is additionally filtered by the FELH0600 light filter and enters through the optical fiber to the PDB450A balanced photodetector. Part of the laser radiation is diverted by the BSN10R semitransparent mirror and fed through the fiber port to the second input of the balanced photodetector. Neutral filters (not shown in the diagram) were used to adjust the intensity, the port setting was used to precisely equalize the signals on the balanced photodetector.

A PLM 520 (520 nm) laser module with multimode fiber output or a Cobolt 06-91 (532 nm) laser with fiber coupling system were used as a source. The best results were obtained with the Cobolt laser, the use of a balanced detection scheme allowed to significantly suppress residual noise of laser intensity.

A synthetic HPHT diamond crystal irradiated with an electron beam with an intensity of 10^{18} electrons per cm^2 and annealed at 800°C, measuring about 300 μm (Fig. 3, *c*) was used to make the sensor. The crystal had a well-defined natural shape, in which case some of the faces correspond to planes perpendicular to the main crystallographic axes of the diamond ($\mathbf{X} = [1, 0, 0]$, $\mathbf{Y} = [0, 1, 0]$ and $\mathbf{Z} = [0, 0, 1]$), and part — planes perpendicular to the axes of species [1,1,1]. The diamond was glued with the face perpendicular to the axis $\mathbf{Z} = [0, 0, 1]$ to the end of the optical fiber, so that the fiber axis approximately coincided with the axis $\mathbf{Z}$ of the diamond. A fiber with a core diameter of 200 μm and a numerical aperture of 0.5 and NOA63 optical adhesive were used. The fiber together with the diamond was fixed inside a brass tube with an inner diameter of 550 μm, slightly larger than the diameter of the fiber sheath (500 μm). A magnetic system consisting of a solenoid creating a scanning magnetic field and two micro-coils creating a bias magnetic field was mounted on the tube. The magnetic system could rotate relative to the tube, allowing the direction of the displacement field to be adjusted. Note that the model can be used to work with other sensors of similar design. In particular, in the case of measurements near a small object, it may be advisable to use a system of large coils surrounding the object, which allows you to get as close as possible to the studied point.

The electronic unit of the model is a custom FPGA board, controlled by a Raspberry Pi 4 Model B microcomputer. The electronic unit allows us to set the necessary current

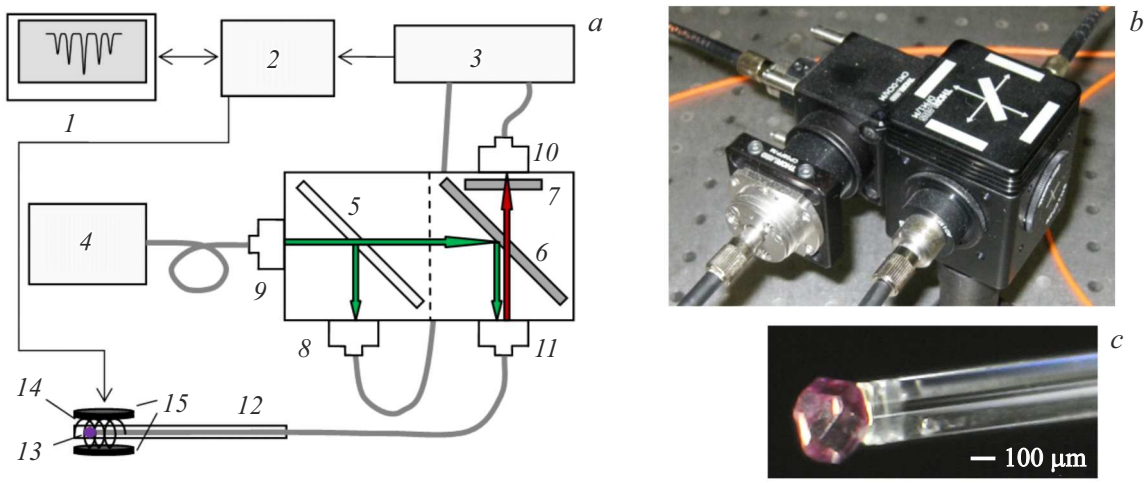

Figure 3. *a* — Model block diagram: *1* — computer, *2* — electronic unit, *3* — balanced photo detector, *4* — laser, *5* — semi-transparent mirror, *6* — dichroic mirror, *7* — filter, *8–11* — collimators, *12* — brass tube, *13* — diamond crystal, *14* — solenoid, *15* — magnetic coils, thick lines show optical fibers; *b* — photograph of the optical part; *c* — diamond crystal glued to the end of the optical fiber.

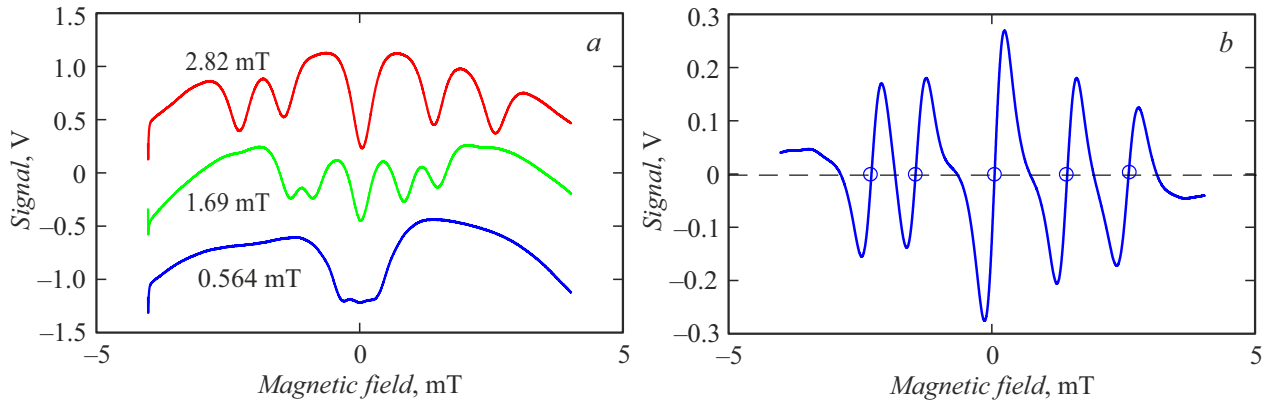

Figure 4. *a* — cross-relaxation resonances in the fluorescence signal at different magnetic displacement fields (the graphs are shifted for clarity); *b* — cross-relaxation resonances after lock-in detection, circles show the centers of resonances.

through the bias coils, constant and alternating components of a given amplitude and frequency of the current through the solenoid, to acquire the photodetector signal synchronously with the alternating component.

To increase the accuracy of measurements in the model, the possibility of lock-in detection of the sensor signal is implemented in the software. The electronic unit is connected to the computer with an Ethernet cable. The client application on the computer is used to select operating modes, set parameters, process and visualize measurement results.

3. Measurement results

The dependence of fluorescence on the z-component of the scanned magnetic field is shown in 4, *a*. The shape of cross-relaxation resonances depends on the direction and magnitude of the magnetic bias field, which are controlled by turning the bias coils and the current through them. All 5 resonances must be well resolved to make measurements. The fully equidistant pattern of the resonances corresponds to a bias field oriented along [2,1,0], but this is not required for measurements. Let us direct the bias field so that the x-component of the displacement field is larger than the y-component, and both are positive, and the distances between the resonances are about the same. For this sensor, cross-relaxation resonances become well resolved at a bias field on the order of $2.5-3$ mT.

Applying a measured magnetic field to the sensor leads to a shift of resonances.

From expressions (7)–(9) it follows that to determine the z-component of the measured field (scalar measurement regime) it is enough only to measure the shift of the central resonance, and using positions of all resonances, it is possible to determine all projections of the measured field (vector regime).

Note that to match the current through the solenoid with the z-component of the scanned field, a calibration measurement is necessary, which can be done by placing the sensor in a known magnetic field. Since we did not set the task of making absolute measurements, we used an approximate calibration done with a calibrated magnetic coil powered from a laboratory current source, if necessary, a more precise calibration can be performed.

Lock-in detection was used to improve the accuracy of measuring the position of the resonances and, consequently, the magnetic field. The shape of cross-relaxation resonances after lock-in detection is shown in 4, *b*. Since the shift of the central resonance allows us to determine the z-component of the measured field, the sensitivity of the magnetometer (in scalar regime) can be defined as the ratio of noise to the slope m of the dependence of the lock-in detector signal on the magnetic field (the derivative of the lock-in detector signal over the magnetic field) in the middle of the central resonance. The magnitude of m at low frequencies is determined by the contrast of the cross-relaxation resonances. When the frequency of the alternating component of the magnetic field used to operate the lock-in detector is increased, a decrease in the response may be observed.

When designing the model, the dependence of the cross-relaxation resonance contrast on the optical pump intensity and the frequency characteristics of the effect were investigated (Fig. 5). The measurements were made in a geometry similar to the model scheme with the difference that the radiation was focused on the diamond crystal using a lens, which allowed for a wider range of intensities.

The maximum contrast corresponded to the intensity of about $100\,\mathrm{W/cm^2}$; when the intensity was increased to several $\mathrm{kW/cm^2}$, a proportional increase in the fluorescence signal with a moderate decrease in contrast was observed. The value of m dropped in the high frequency range, the cutoff frequency on the level 0.5 at low intensity was 0.5 kHz and increased with increasing intensity. Based on this research, the model was designed to work with frequencies of the alternating magnetic field component in the range of $0.5-10$ kHz.

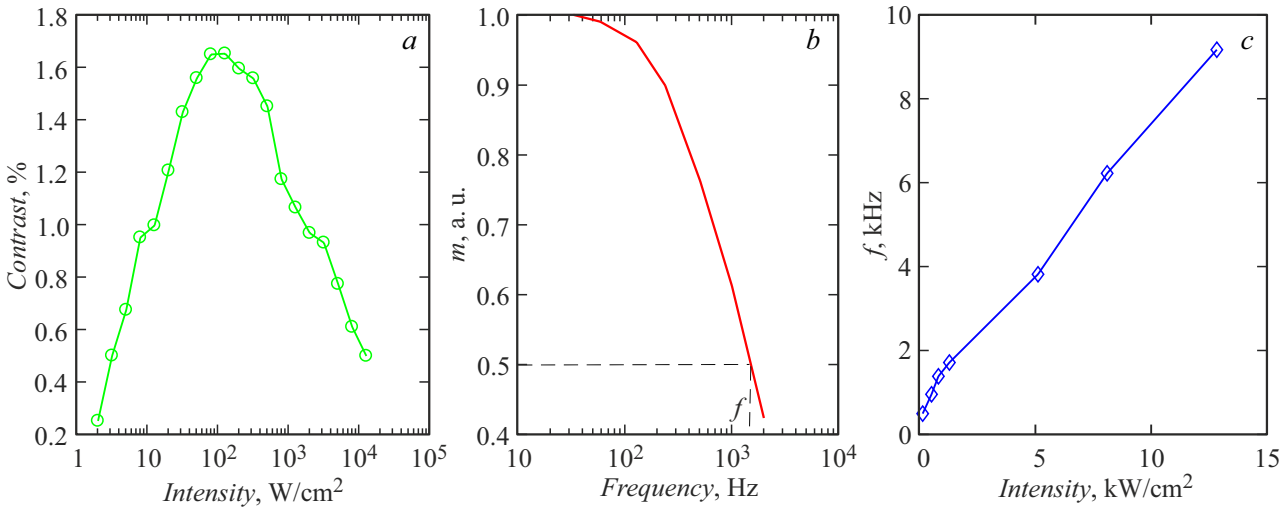

Figure 5. *a* — contrast dependence on intensity; *b* — the slope of the lock-in signal dependence on the magnetic field at the resonance center as a function of the frequency the slope of the variable component of the magnetic field (intensity 0.8 kW/cm^2); *c* — the cutoff frequency on the level 0.5, depending on the pump intensity.

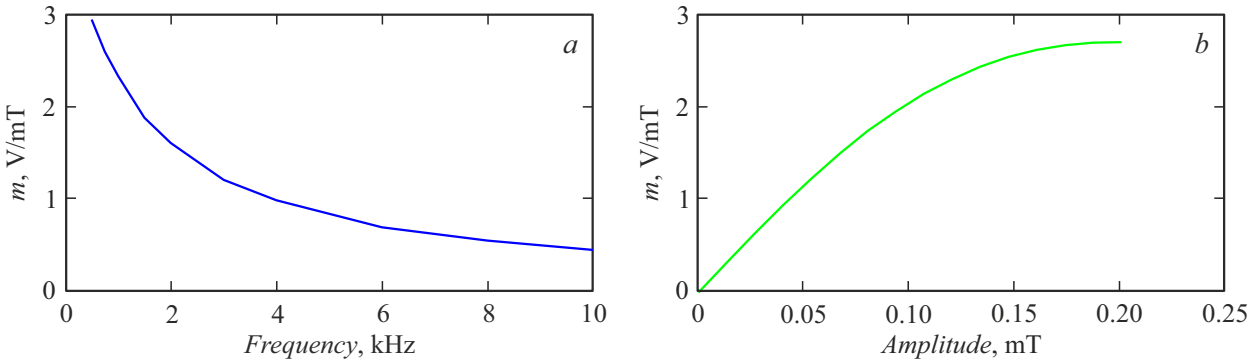

Figure 6. The slope of the lock-in signal dependence on the magnetic field at the resonance center as a function of the frequency (*a*) and amplitude (*b*) of the variable magnetic field component.

In the sensor we used, the laser power was limited by overheating of the diamond sample, leading to the destruction of the adhesive layer. Stable operation was possible at the radiation power of 15 mW, which corresponds to the intensity of 50 W/cm^2. At this intensity, the value m decreased with increasing the frequency of the alternating component of the magnetic field (Fig. 6, *a*). The noise was almost independent of the frequency in the range of the model operation, with distinctive peaks at 0.5 and 1 kHz, related to the peculiarities of the Cobolt 06-91 laser used (when working with the PLM 520 laser no such peaks were observed, but the total noise level was higher). To work with the sensor we selected the frequency 0.75 kHz, providing the best sensitivity, and amplitude 0.16 mT, close to the optimal (Fig. 6, *b*), under these conditions $m = 2.6$ V/mT.

To measure the noise characteristics of the magnetometer and to determine the sensitivity (in scalar regime), we used a technique similar to the one used in [10,11]. The value of the scanned magnetic field corresponding to the middle of the central resonance was set. The consecutive values of the lock-in detector signal were recorded. The square root of the spectral density normalized by m was calculated. The results of measurements with the time constant of the lock-in detector (time of measurement of each point) $\tau = 0.1$ s and the number of points 10 000 (total length of the record 1000 s) are shown in Fig. 7. The average noise at frequencies greater than 0.6 Hz is 18 nT/Hz$^{1/2}$. The greater noise at low frequencies, corresponding to the slow drift of the lock-in detector signal with a characteristic time on the order of a second or more, which was also observed in the temporal shape of the signal, may be related to changes in the magnetic field in the laboratory. To test this assumption, noise measurements were made when the sensor was partially shielded with a steel screen providing about a tenfold reduction in the magnetic field. We observed a significant decrease in the drift of the lock-in detector signal, and the magnitude and nature of the noise at frequencies greater than 0.6 Hz practically did not change. Thus, the magnetic field sensitivity in the scalar regime with the sensor used can be estimated as 18 nT/Hz$^{1/2}$.

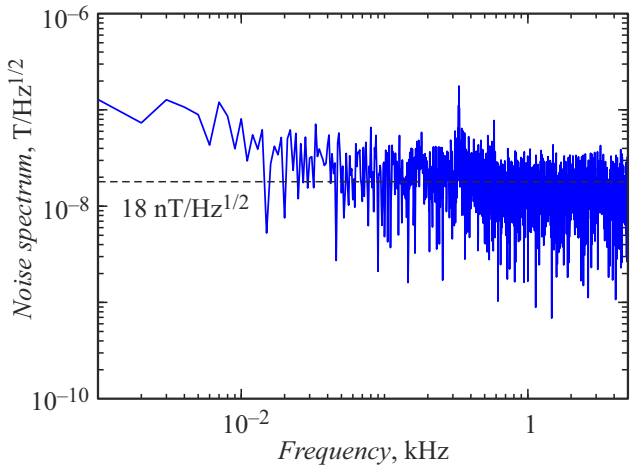

Figure 7. Noise spectrum of the magnetometer.

The maximum sensitivity, limited by the photocurrent shot noise, can be estimated as $\sigma = \sqrt{2qI}K/m$, where I — photocurrent, q — electron charge, $K = 10^7$ V/A — gain of the balanced photodetector amplifier, which under measurement conditions (photocurrent $12.3\,\mu$A, corresponds to fluorescence power $27\,\mu$W) is 7.6 nT/Hz$^{1/2}$. For the balanced optical signal detection scheme used in the model, which allows to significantly reduce the influence of the laser intensity noise, the shot noise power doubles and, accordingly, the maximum sensitivity is $2^{1/2}$ times worse and is 10.7 nT/Hz$^{1/2}$. Thus, the achieved sensitivity is only 1.7 times inferior to the maximal possible sensitivity.

To measure the magnetic field, an iterative procedure is implemented in the model to find the positions of the centers of the resonances (corresponding to the zero signal of the lock-in detector). Each step of the iterative procedure sets the value of the constant component of the scanned field b_n, corresponding to the center of the resonance calculated in the previous step, measures the lock-in detector signal, and calculates the new value of the resonance position in the linear approximation:

$$b_{n+1} = b_n - f_n/m,$$

where m — the slope at the center of the corresponding resonance.

In the scalar regime only the position of the central resonance is measured, in the vector regime — the position of each resonance is calculated in turn at each measurement step. The positions of the resonance centers in the absence of the measured field can be used as initial values; the measurement range in this case is determined by the width of the cross-relaxation resonances and is $(-200)-(+200)\,\mu$T for each projection. The values of m are determined before starting the iterative procedure and do not change during measurement.

To check the iterative procedure and determine the sensitivity in this regime, test measurements were carried out. For scalar measurements, a magnetic coil powered by an Agilent 33250A generator created a square-wave magnetic field with an amplitude of $12\,\mu$T and a period of 10 s; in the vector mode, a rectangular pulse of 25 s, generated by the same coil placed at an angle to the sensor, was used. The measurements showed (Fig. 8) that it takes 1−2 iterative steps to establish the measurement result; rapid changes in the magnetic field can lead to outlier measurement results with the duration of one iteration. The noises in the scalar regime, estimated from the signal on the square-wave top, agree with the results obtained above. The vector regime requires determining the positions of 5 resonances, which increases the time required to measure each point by 5 fold.

4. Discussion. Possible ways to increase sensitivity

The achieved sensitivity of 18 nT/Hz$^{1/2}$ is not among the best for magnetometry using NV-centers in diamond, including methods without microwave radiation. In particular, work [11] demonstrated sensitivity of 0.3 nT/Hz$^{1/2}$. However, the method used in [11] requires the application of a strong (on the order of 0.1 T) and precisely oriented magnetic field to the diamond, which complicates the sensor construction and limits the applicability of the magnetometer. In addition, high sensitivity was obtained using isotopically pure diamond with ^{12}C 99.97%, in studies with diamond with natural isotope content the sensitivity was 6 nT/Hz$^{1/2}$ [10] at a higher (~ 200 mW) pump intensity. A more feasible approach for creating microscopic sensors without microwave radiation is based on driving diamond with NV-centers with HF radiation (1−10 MHz) [12]. For a sensor with similar design and parameters to ours, the stated sensitivity limited by shot noise is 3.6 nT/Hz$^{1/2}$, and determined by the observed noise 4−5 times worse. This is comparable to the sensitivity we demonstrated without the need for HF radiation.

Note, that the sensitivity we achieved is only 1.7 times lower than the maximum sensitivity limited by the shot noise, so that the possibility of increasing the sensitivity by optimizing the electronic part is practically exhausted.

A natural way to increase the sensitivity limit is to increase the fluorescence intensity and correspondingly the photocurrent at the detector, which can be achieved by increasing the pump intensity or by increasing the fluorescence collection efficiency. If the heat sink problems are solved, it is possible to increase the pump intensity by at least an order of magnitude without significantly reducing the contrast of the resonances. Various methods are used to increase the collection of fluorescence. In work [12], for example, using a larger diameter fiber and a reflective coating, the resulting photocurrent value ($\sim 40\,\mu$A) is about three times higher than what we obtained with a similar diamond crystal and pump intensity. Even more promising could be the use of special parabolic condenser [17]. It is also possible to place the photodetector close to the crystal

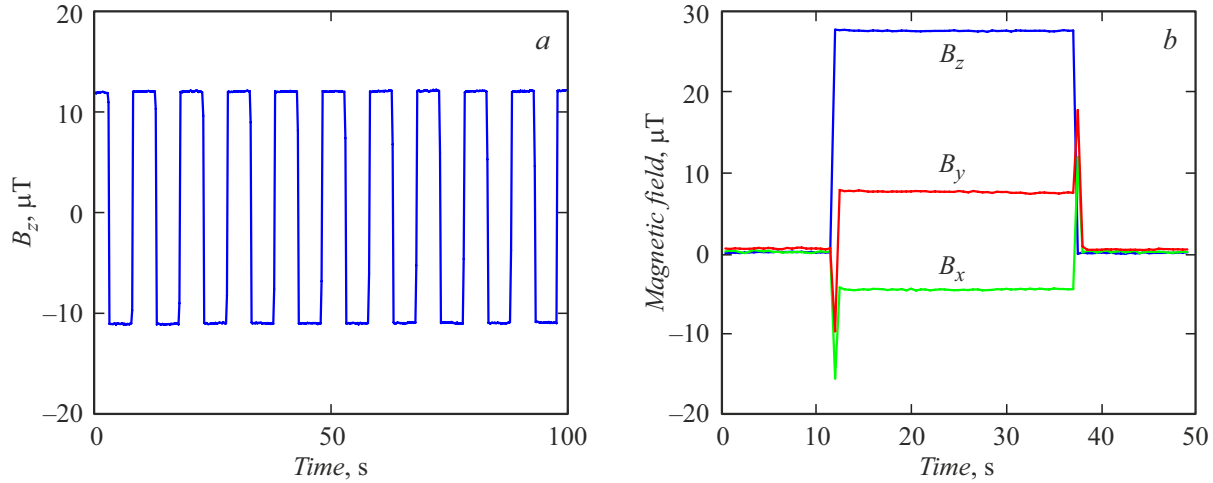

Figure 8. Magnetic field measurement: *a* — scalar regime, square-wave, *b* — vector regime, rectangular pulse.

(see, for example, [6]) and/or to increase the size of the active element, which, however, would increase the size of the sensor.

Another way to increase the sensitivity could be to increase the contrast of the cross-relaxation resonances by increasing the concentration of NV-centers. In the available samples (maximum irradiation dose 10^{18} electrons on cm^2) we observed an increase in contrast with increasing dose without broadening of the resonances. Thus, one can hope for a further increase in sensitivity with increasing concentration.

The use of isotopically pure diamond could potentially be of interest for narrowing the cross-relaxation resonances and increasing sensitivity, but, as far as we know, cross-relaxation resonances in such samples have not been investigated. In addition, the sample itself, along with the low content of ^{13}C, must have a sufficient concentration of NV-centers to observe cross-relaxation resonances.

Another way to increase sensitivity would be to use a magnetic flux concentrator [18], but this method would inevitably lead to a decrease in spatial resolution.

Conclusion

A model of a new type of optical quantum magnetometer based on cross-relaxation resonances in an ensemble of NV-centers in diamond was created. A diamond crystal of the size of about 300 μm, attached to the end of the optical fiber was used as the sensor. The magnetometer does not use microwave radiation used in traditional magnetometry scheme with NV-centers, and allows both scalar (one projection) and vector magnetic field measurement. In scalar regime, sensitivity to magnetic field 18 $nT/Hz^{1/2}$ has been demonstrated.

Acknowledgments

The authors are grateful to V.L. Velichansky and A.O. Levchenko for the provided diamond crystals.

Funding

We acknowledge the support by Center of Excellence „Center of Photonics“ funded by The Ministry of Science and Higher Education of the Russian Federation, contract № 075-15-2022-316.

Conflict of interest

The authors declare that they have no conflict of interest.

References

[1] L. Rondin, J.-P. Tetienne, T. Hingant, J.-F. Roch, P. Maletinsky, V. Jacques. Rep. Prog. Phys., **77** (5), 056503 (2014). DOI: 10.1088/0034-4885/77/5/056503
[2] J.F. Barry, J.M. Schloss, E. Bauch, M.J. Turner, C.A. Hart, L.M. Pham, R.L. Walsworth. Rev. Mod. Phys., **92**, 015004 (2020). DOI: 10.1103/RevModPhys.92.015004
[3] J.L. Webb, J.D. Clement, L. Troise, S. Ahmadi, G.J. Johansen, A. Huck, U.L. Andersen. Appl. Phys. Lett., **114**, 231103 (2019). DOI: 10.1063/1.5095241
[4] R.L. Patel, L.Q. Zhou, A.C. Frangeskou, G.A. Stimpson, B.G. Breeze, A. Nikitin, M.W. Dale, E.C. Nichols, W. Thornley, B.L. Green, M.E. Newton, A.M. Edmonds, M.L. Markham, D.J. Twitchen, G.W. Morley. Phys. Rev. Appl., **14**, 044058 (2020). DOI: 10.1103/PhysRevApplied.14.044058
[5] K. Huang, Y. Nie, B. Du, J. Jiang, Z. Zhang, Q Wang, R. Xu. Appl. Phys. Lett., **119**, 114005 (2021). DOI: 10.1063/5.0061156
[6] F.M. Stürner, A. Brenneis, T. Buck, J. Kassel, R. Rölver, T. Fuchs, A. Savitsky, D. Suter, J. Grimmel, S. Hengesbach, M. Förtsch, K. Nakamura, Hi. Sumiya, S. Onoda, J. Isoya, F. Jelezko. Adv. Quantum Technol., **4** (4), 2000111 (2021). DOI: 10.1002/qute.202000111

[7] L. Rondin, J.-P. Tetienne, P. Spinicelli, C.D. Savio, K. Karrai, G. Dantelle, A. Thiaville, S. Rohart, J.-F. Roch, V. Jacques. Appl. Phys. Lett., **100**, 153118 (2012). DOI: 10.1063/1.3703128
[8] D.A. Simpson, J.-P. Tetienne, J.M. McCoey, K. Ganesan, L.T. Hall, S. Petrou, R.E. Scholten, L.C.L. Hollenberg. Sci. Rep., **6**, 22797 (2016). DOI: 10.1038/srep22797
[9] R. Staacke, R. John, R. Wunderlich, L. Horsthemke, W. Knolle, C. Laube, P. Glösekötter, B. Burchard, B. Abel, J. Meijer. Adv Quantum Technol., **3**, 2000037 (2020). DOI: 10.1002/qute.202000037
[10] A. Wickenbrock, H. Zheng, L. Bougas, N. Leefer, S. Afach, A. Jarmola, V.M. Acosta, D. Budker. Appl. Phys. Lett., **109**, 053505 (2016). DOI: 10.1063/1.4960171
[11] H. Zheng, Z. Sun, G. Chatzidrosos, C. Zhang, K. Nakamura, H. Sumiya, T. Ohshima, J. Isoya, J. Wrachtrup, A. Wickenbrock, D. Budker. Phys. Rev. Appl., **13**, 044023 (2020). DOI: 10.1103/PhysRevApplied.13.044023
[12] A.K. Vershovskii, A.K. Dmitriev. Tech. Phys., **65** (8), 1301 (2020). DOI: 10.1134/S1063784220080216
[13] R.A. Akhmedzhanov, L.A. Gushchin, I.V. Zelensky, V.A. Nizov, N.A. Nizov, D.A. Sobgaida. Opt. Spectr., **127** (2), 260 (2019). DOI: 10.1134/S0030400X19080034
[14] V.M. Acosta, K. Jensen, C. Santori, D. Budker, R.G. Beausoleil. Phys. Rev. Lett., **110**, 213605 (2013). DOI: 10.1103/PhysRevLett.110.213605
[15] R. Akhmedzhanov, L. Gushchin, N. Nizov, V. Nizov, D. Sobgayda, I. Zelensky, P. Hemmer. Phys. Rev. A, **96**, 013806 (2017). DOI: 10.1103/PhysRevA.96.013806
[16] R. Akhmedzhanov, L. Gushchin, N. Nizov, V. Nizov, D. Sobgayda, I. Zelensky, P. Hemmer. Phys. Rev. A, **100**, 043844 (2019). DOI: 10.1103/PhysRevA.100.043844
[17] G. Chatzidrosos, J.S. Rebeirro, H. Zheng, M. Omar, A. Brenneis, F.M. Stürner, T. Fuchs, T. Buck, R. Rölver, T. Schneemann, P. Blúmler, D. Budker, A. Wickenbrock. Front. Photon., **2**, 732748 (2021). DOI: 10.3389/fphot.2021.732748
[18] I. Fescenko, A. Jarmola, I. Savukov, P. Kehayias, J. Smits, J. Damron, N. Ristoff, N. Mosavian, V.M. Acosta. Phys. Rev. Res., **2**, 023394 (2020). DOI: 10.1103/PhysRevResearch.2.023394